Optimizing the Fluorescence Properties of Nanoemulsions for Single Particle Tracking in Live Cells

Xinyue Wang, Nicolas Anton, Ashokkumar Pichandi, Halina Anton, Tkhe Kyong Fam, Thierry Vandamme, Andrey Klymchenko, Mayeul Collot

Optimizing the Fluorescent Properties of Nano-emulsions for Single Particle Tracking in Live Cells

Xinyue Wang,[a] Nicolas Anton,[a,*] Pichandi Ashokkumar,[b] Halina Anton,[b] Tkhe Kyong Fam,[b] Thierry Vandamme,[a] Andrey S. Klymchenko,[b,*] Mayeul Collot [b,*]

[a] Université de Strasbourg, CNRS, CAMB UMR 7199, F-67000 Strasbourg, France

[b] Laboratory of Biophotonic and Pathologies, CNRS UMR 7021, Université de Strasbourg, Faculté de Pharmacie, 74, Route du Rhin, 67401 Illkirch, France

KEYWORDS. Lipid nanoparticles, nano-emulsions, dioxaborine, two-photon imaging, single particle tracking.

ABSTRACT: Nano-emulsions (NEs) are biocompatible lipid nanoparticles composed of an oily core stabilized by a surfactant shell. It is acknowledged that the surface decoration with poly(ethylene glycol) (PEG), through the use of non-ionic surfactants, confers a high stealth in biological medium with reduced non-specific interactions. Tracking individual NEs by fluorescence microscopy techniques would lead to a better understanding of their behavior in cells and thus require the development of bright single particles with enhanced photostability. However, the understanding of the relationship between the physicochemical properties and chemical composition of the NEs, on the one hand, and its fluorescence properties of encapsulated dyes, on the other hand, remains limited. Herein, we synthesized three new Dioxaborine Barbituryl Styryl dyes (DBS) that displayed high molar extinction coefficients (up to 120,000 $M^{-1}.cm^{-1}$) with relatively low quantum yields in solvents and impressive fluorescence enhancement when dissolved in viscous oils (up to 0.98). The reported screening of 9 different oils allowed disclosing a range of efficient "oil/dye" couples, and understanding the main parameters that lead to the brightest NEs. We determine vitamin E acetate / DBS-C_8 as the representative most efficient couple combining high dye loading capabilities and low aggregation induced quenching leading to <50 nm ultrabright NEs (as high as 30×10^6 $M^{-1}.cm^{-1}$) with negligible dye leakage in biological media. Beyond a comprehensive optical and physicochemical characterization of fluorescent NEs, cellular two-photon excitation imaging was performed with polymer-coated cell penetrating NEs. Thanks to their impressive brightness and photostability, NEs displaying different charge surfaces were microinjected in HeLa cells and were individually tracked in the cytosol in order to study their relative velocity.

Introduction

A great variety of nanocarriers of drugs and contrast agents has been developed to date in nanomedicine[1, 2, 3, 4] notably those based on mesoporous silica[5, 6] semiconductors,[7] gold or iron oxide[8] as well as organic materials, such as dendrimers,[9, 10] polymers,[11, 12, 13, 14, 15] lipids (including liposomes[16] and solid lipid naoparticles[17]). Although the current organic nanocarriers are dominated by the well-established polymer and lipid nanoparticles, nano-emulsions (NEs) that are composed of an oily core stabilized by surfactants, are rapidly emerging in the last ten years.[18, 19, 20] They are promising vehicle for a functional cargo owing to their low toxicity, high encapsulation efficiency, simple fabrication methods, and finally (and not least), very high stability compared to microscale emulsions. Interestingly, the use of a highly PEGylated surfactant (e.g. Kolliphor ELP®, that decorate the droplets with a Mw 1500 PEG chain) leads to drastically reduce their non-specific interaction with cells[21, 22, 23] as well as increasing the circulation time in blood before complete clearance.[24, 25] In addition, intrinsically related to their formulation process, the NEs size and surface properties can be very finely tuned and adapted to given specifications. It follows therefrom that encapsulating lipophilic fluorescent probes in such oily NEs gives rise to fluorescent NEs, that are valuable tools in bioimaging – as compatible with various accessible fluorescence imaging techniques.[26, 27, 28] This study aims at understanding, on an empirical point of view, the relationship existing between the nature of oil, the chemical structure of fluorescent probe, and the physicochemical properties of the NEs (see graphical abstract). Regarding the oil, the main required property is its ability to form stable NEs. However several other parameters like hydrophobicity, polarity, and viscosity could greatly influence not only the physicochemical properties of the NEs itself but also the photophysical properties of the encapsulated fluorophore, thus leading to important changes in the fluorescence properties of the NEs.

The encapsulated fluorophores have to fulfill several requirements: 1) They should be well solubilized in oil in order to reach high dye loading; 2) They should be sterically bulky enough to prevent aggregation caused quenching (ACQ)[29] that would limit the quantum yield of the NEs and therefore their brightness; 3) The dye should be hydrophobic enough not to escape from the NEs[21] and 4) it should be photostable enough to allow tracking of the NEs over the time. As fluorophores, cationic carbocyanines bearing long hydrocarbon chains were used for this purpose.[27, 30] Our group improved this approach by combining those cyanines with bulky hydrophobic tetraphenyl borate counterions that led to brighter NEs due to two synergic effects[26] : (i) enhancing hydrophobicity and thus allowing higher dye loading percentage, and (ii) preventing ACQ by the bulkiness of the counter ion.[31] The obtained NEs were successfully used for tracking single NEs in zebrafish embryo[26] and for monitoring their integrity in the bloodstream and tumor in the living mice.[28] Although this approach led to bright NEs, the use of borate counter-ions can lead to cytotoxic effects,[32] which can be detrimental for the cellular or *in vivo*

studies. Non-charged fluorophores can circumvent this issue, as they can be sufficiently hydrophobic to be dissolved in oil without any other additive. Nile red (NR) is a non-charged solvatochromic dye that is commonly used to stain the cellular lipid droplets[33] and to fluorescently label NEs. However, it was shown that, due to insufficient lipophilicity, Nile Red undergoes rapid leakage in biological media.[21] To prevent the dye leakage a hydrophobic version of NR, NR668 (Figure 1), bearing three alkyl chains was developed and successfully loaded in NEs providing bright particles.[21] Even though NR668 constitutes a valuable tool for making fluorescent NEs,[25 34] there is still a room for improvement as it has a limited brightness with a molar extinction coefficient of 45,000 $M^{-1}.cm^{-1}$. Also, NR derivatives can suffer from limited photostability and their broad absorption and emission spectra are detrimental in multicolor bioimaging when combined with additional fluorophores or fluorescent proteins.[35] In addition, a systematic study on the effect of oil and fluorophore nature on the fluorescence characteristics of dye-loaded nanoemulsions is still missing. In order to circumvent these limitations, we got interested in dioxaborine-fluorophores as they were shown to be efficient to develop bright fluorescent nanomaterials.[36, 37, 38] We recently introduced a new family of fluorophores called StatoMerocyanines composed of an indolenine moiety and a bulky barbiturate stabilized by a dioxaborine complex (Figure 1). These fluorogenic dyes display ultrabright fluorescence in oil and were used as lipid droplets markers in cellular and tissue imaging.[35] Although Statomerocyanines are bright in oil, the one compatible with common 488 nm laser excitation, namely SMCy3, was limited by modest quantum yield (0.25). In order to obtain a fluorophore absorbing in this range and with enhanced fluorescence properties, we conserved the barbituryl dioxaborine moiety and replaced the indolenine part by aniline donors to give rise to hemicyanine like fluorophores (also called styryl dyes, figure 1) that we named Dioxaborine Barbituryl Styryl dyes (DBS). These new dyes displayed interesting properties for NEs loading and were compared to NR668. This study led to ultrabright NEs with improved photo-physical properties that were highly suitable for tracking individual NEs in cells.

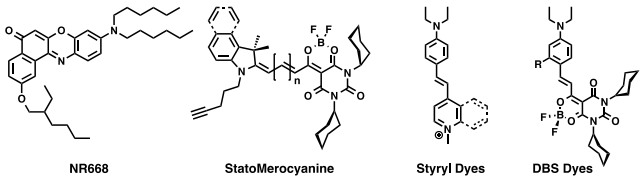

Figure 1. Structure of the different fluorophores discussed in this work

Materials and methods

Materials. Labrafac WL® 1349 (medium chain triglycerides, MCT) was obtained from Gattefossé (Saint-Priest, France), Vitamin E acetate (VEA) was purchased from Tokyo Chemical Industry (Tokyo, Japan). All the other oils used for spectra study are of chemical grade except colza oil, which is of food grade. The surfactant, Kolliphor ELP®, was from BASF (Ludwigshafen, Germany). Poly(maleic anhydride-alt-a-octadecene) (PMAO) was purchased from Sigma Aldrich (St. Louis, USA). NR668 is a homemade modified Nile Red fluorophore.[21] Phosphate buffered saline (PBS) was from Eurobio (Gourtaboeuf, France) and fetal bovine serum (FBS) from Lonza.

Synthesis. All starting materials for synthesis were purchased from Alfa Aesar, Sigma Aldrich or TCI Europe and used as received unless stated otherwise. NMR spectra were recorded on a Bruker Avance III 400 MHz spectrometer. Mass spectra were obtained using an Agilent Q-TOF 6520 mass spectrometer. Synthesis of all new compounds is described in the supporting information.

Spectroscopy. The water used for spectroscopy was Milli-Q water (Millipore), all the solvents were spectro grade. Absorption and emission spectra were recorded on a Cary 400 Scan ultraviolet–visible spectrophotometer (Varian) and a Fluoro-Max-4 spectrofluorometer (Horiba Jobin Yvon) equipped with a thermostated cell compartment, respectively. For standard recording of fluorescence spectra, the emission was collected 10 nm after the excitation wavelength. All the spectra were corrected from wavelength-dependent response of the detector. Quantum yields were determined by comparison with: Rhodamine 6G in water[39] as reference using the following equation:

$$\mathrm{QY} = \mathrm{QY}_R \times \frac{I \times OD_R \times n^2}{I_R \times OD \times n_R^2}$$

where QY is the quantum yield, I is the integrated fluorescence intensity, n is the refractive index, and OD is the optical density at the excitation wavelength. R represents the reference.

Solubility of DBS dyes in oils. An excess amount of dye was weighted, firstly, dissolved in acetone to obtain a stock solution, and then, was added to an appropriate amount of oil quickly. Next, oil solution was heated to 60 °C and vortexed to homogeneousness. After that, acetone was evaporated to get a saturated oil solution and then centrifuged. Lastly, upper oil solution was taken and diluted in dioxane by 50 times for the absorption test. DBS-H, DBS-OH and DBS-C_8 were tested in labrafac, castor oil and VEA respectively. The solubility percentage was calculated as following:

$$\mathrm{S}\ (\%) = \frac{OD \times 50 \times 1\ mL \times MW}{\varepsilon_{dioxane} \times m} \times 100$$

Where OD is the optical density, 50 is the dilution factor, 1 mL is the final volume after dilution used for the absorption test, MW is the molar weight of the dye, $\varepsilon_{\mathrm{dioxane}}$ is the molar extinction coefficient of the dye in dioxane and m is the weight of saturated dye-oil solution.

TPE measurements and TPE imaging. Two-photon absorption cross-section measurements were performed using Rhodamine 6G in methanol as a calibration standard according to the method of Webb *et al.*[40] Two-photon excitation was provided by an InSight DS+ laser (Spectra Physics) with a pulse duration of 120 fs. The laser was focused with an achromatic lens (f = 2 cm) in a cuvette containing the dye (DBS-H: 16 μM, DBS-OH: 28 μM, DBS-C_8: 18 μM and NR668: 10 μM) in dioxane and the spectra were recorded with a fibered spectrometer (Avantes) by collecting the fluorescence emission at 90° with a 20 × Olympus objective. Two-photon fluorescence microscopy imaging was performed by using a home-built two-photon laser scanning setup based on an Olympus IX70

inverted microscope with an Olympus 60 × 1.2NA water immersion objective.[41] Two-photon excitation was provided by an InSight DS+ laser (Spectra Physics, 80 MHz, 120 fs) with an excitation power around 5 mW (930 nm for DBS-C_8, 910 nm for NR668 and 750 nm for Hoechst), and photons were detected with Avalanche Photodiodes (APD SPCM-AQR-14-FC, Perkin-Elmer) connected to a counter/timer PCI board (PCI6602, National Instrument). Imaging was carried out using two fast galvo mirrors in the descanned fluorescence collection mode. Images corresponding to the blue (Hoechst) and green (DBS-C_8 and NR668 dye) channels were recorded simultaneously using a dichroic mirror (Beam splitter 495 nm DCXR) and two APDs. Typical acquisition time was 50 s. Since the excitation of Hoechst stain at 910 and 930 nm in our experimental conditions did not yield a good quality image, we used 750 nm excitation for Hoechst and independent images were taken for blue and green channel and then processed with ImageJ.

X-ray crystallography. Single crystals of DBS-C_8 were obtained by solvent exchange method using DCM as solvent and cyclohexane as antisolvent.[42] X-Ray diffraction data collection was carried out on a Bruker APEX II DUO Kappa-CCD diffractometer equipped with an Oxford Cryosystem liquid N2 device, using Mo-Kα radiation (λ = 0.71073 Å). The crystal-detector distance was 38mm. The cell parameters were determined (APEX2 software)[43] from reflections taken from tree sets of 12 frames, each at 10s exposure. The structure was solved by Direct methods using the program SHELXS-2013.[44] The refinement and all further calculations were carried out using SHELXL-2013.[45] The H-atoms were included in calculated positions and treated as riding atoms using SHELXL default parameters. The non-H atoms were refined anisotropically, using weighted full-matrix least-squares on F2. A semi-empirical absorption correction was applied using SADABS in APEX2;[43] transmission factors: Tmin/Tmax = 0.6697/0.7456.

Cytotoxicity assay. Cytotoxicity assay of the DBS dyes and NR668 was quantified by the MTT assay (3-(4,5-dimethylthiazol-2-yl)-2,5-diphenyltetrazolium bromide). A total of $1x10^4$ HeLa (ATCC® CCL-2™) cells/well were seeded in a 96-well plate 24 h prior to the cytotoxicity assay in Dulbecco's Modified Eagle Medium (Gibco Lifetechnologies -DMEM) complemented with 10% fetal bovine serum, Gentamicin (100 µg/mL), L-Glutamine (2 mM), non-essential amino acids (1 mM), MEM vitamin solution (1%) and were incubated in a 5% CO_2 incubator at 37°C. After medium removal, an amount of 100 µL DMEM containing 5 µM, 1 µM or 0.2 µM of DBS dye (DBS-H, DBS-OH, DBS-C_8) or NR668 was added to the cells and incubated for 24 h at 37°C (5% CO_2). As control, for each 96-well plate, the cells were incubated with DMEM containing the same percentage of dioxane (0,5% v/v) as the solution with the tested dyes or with triton X-100 0.1% as a positive control of cytotoxicity. After 24h of a dye incubation, the medium was replaced by 100 µL of a mix containing DMEM + MTT solution (diluted in PBS beforehand) and the cells were incubated for 4 h at 37°C. Then, 75 µL of the mix was replaced by 50 µL of DMSO (100%) and gently shaken for 15 min at room temperature in order to dissolve the insoluble purple formazan reduced in the living cells. The absorbance at 540 nm was measured (absorbances of the dyes at 540 nm were taken into account). Each concentration of dye was tested in sextuplicate in 3 independent assays. For each concentration, we calculated the percentage of cell viability in reference of the control DMEM+ 0.5% dioxane.

Formulation and characterization of nano-emulsions. Nano-emulsions (NEs) were formulated with spontaneous emulsification method, as described previously.[34] Firstly, the dye was dissolved in a proper amount acetone and then added to the oil (80°C) quickly. After the system was mixed homogeneously, acetone was evaporated at 80°C for several hours and then at room temperature overnight. Next, the surfactant was added, and the mixture was homogenized at 80°C. With the addition of milli Q water (or PBS for the cell experiments), NEs were formed under vortex. Different surfactant-oil ratios (SOR)[41] were selected for different oils. In order to promote the penetration of NEs into cells, PMAO was used as an interface-active polymer, which is dissolved in the oil before all the steps.[34] After the formulation, size and ξ potential of all the NEs were tested by Dynamic Light Scattering with the instrument Zetasizer® (Malvern, UK). For the size measurement, all the emulsions were diluted by 100 times and measured at a temperature of 25°C. Both size distribution and polydispersity index (PDI) were recorded. For the ξ potential measurement, emulsions with PMAO and without PMAO using PBS were tested after 1 h to ensure the sufficient hydrolysis of PMAO at the interface, with a dilution factor of 1,000.

Photostability Test. NEs with 1% dye loading were chosen for the photostability test. All the NEs were diluted to keep the dye concentration at 1 µM in the final solutions. In order to make sure that all the NEs were excited at the same ε (40,000 $M^{-1}.cm^{-1}$), 520 nm was chosen as the excitation wavelength for NR668 NEs, while 490 nm was chosen for DBS-H/DBS-OH/DBS-C_8 NEs. Emission signal was monitored at 600 nm for all fluorophores. The measurement was conducted for 1 h. A relative fluorescent intensity (%) was normalized to the maximum intensity at the starting point.

Fluorescence Correlation Spectroscopy (FCS). FCS measurements were performed on a home-built confocal set-up based on a Nikon inverted microscope with a Nikon 60x 1.2NA water immersion objective.[47] Excitation was provided by a cw laser diode (532 nm, Oxxius) and photons were detected through a bandpass 580/84 nm filter (Semrock) with a fibered Avalanche Photodiode (APD SPCM-AQR-14-FC, Perkin Elmer) connected to an on-line hardware correlator (ALV7000-USB, ALV GmbH, Germany). Typical acquisition time was 5 min (10 × 30 s) with an excitation power of 0.5 mW at the sample level. The data were analyzed using the PyCorrFit software.[48] 100-times diluted NEs for the size measurement were used for FCS study. Before measurement, another 100-fold dilution was performed to all the samples respectively in PBS and 10% FBS + 90% PBS solutions. Different dye-loaded NEs (0.2%, 1.0% and 2.5% loading in oil) of two dyes (DBS-C_8 and NR668) were used for a comparison. 50 nM solution of 6-carboxytetramethylrhodamine (TMR) in water was used as a reference. 200 µL of each samples were placed in a 96-well plate. The measurement ran 10 seconds and 15 times for each NEs sample.

Cellular imaging. HeLa cells (ATCC® CCL-2™) were grown in Dulbecco's Modified Eagle Medium without phenol red (DMEM, Gibco-Invitrogen) supplemented with 10% fetal bovine serum (FBS, Lonza), 1% L-Glutamine (Sigma Aldrich) and 0.1% antibiotic solution (gentamicin, Sigma-Aldrich) at 37°C in humidified atmosphere containing 5% CO_2. Cells were seeded onto a 35 mm glass-bottomed imaging dish

(IBiDi®) at a density of 5×10^4 cells/well 24 h before the microscopy measurement. For imaging, the culture medium was removed and the attached cells were washed with Opti-MEM (Gibco–Invitrogen). Next, the cells were incubated in Opti-MEM with Hoechst (5 µg/mL) to stain the nuclei, the living cells were washed twice with Opti-MEM and visualized in Opti-MEM. The solutions of NEs were placed in a femtotip II (Eppendorf) at a dye concentration of 3 µM and were microinjected using a Femtojet® 4i device (Eppendorf), parameters: Pi=90 [hPa]; Ti=0.3 [s]; Pc=10 [hPa]. Right after micro injection video of the cell was acquired with an integration time of 50 ms for 30 s (600 frames), then multicolor pictures were taken followed by a second movie (5 min post injection). The images were acquired with a Nikon Ti-E inverted epifluorescence microscope, equipped with CFI Plan Apo × 60 oil (NA = 1.4) objective, and a Hamamatsu Orca Flash 4 sCMOS camera. The acquisition settings were: Hoechst (ex. 395 nm, em. 475±50 nm), DBS-loaded NEs (ex. 470 nm, em. 531±40 nm). The images were recorded using NIS Elements and then processed with Icy software. For TPE imaging, the cells were incubated with NEs in Opti-MEM for 2 hrs at 37°C then with Hoechst (5 µg/mL) for 15 min to stain the nuclei and images were taken from home-built two-photon laser scanning microscope (*vide supra*).

Tracking of individual NEs. The movies were acquired at 20 Hz for the total duration of 30 s. The tracking analysis was performed using Imaris 9.2.1 software (Bitplane Inc.) Individual fluorescent foci were identified in each frame and the fluorescent spots in different frames were joined to form trajectories if the centroid positions of the spots were within 500 nm between subsequent frames. Trajectories that lasted ten frames or longer were kept for subsequent analysis. To calculate the velocity of each spot the displacement between the subsequent frames was divided by the acquisition time (50 ms). For each type of NEs, 3 cells were analyzed with roughly 1000 trajectories and $2\text{-}4\times10^4$ displacements detected in each cell. The mean fluorescence intensity of the single NEs in the time-lapse images was measured by using Image J software. Five images, corresponding to t1 =0s, t2 = 1.5s, t3=3s, t4 = 4.5s and t5=6 s were analyzed. The time interval of 1.5 s between the analyzes was chosen in order to ensure the turnover of the NEs. A threshold was then applied to the images to isolate the fluorescent spots corresponding to NEs from the fluorescent background. Then, a particle analysis function was used to identify their borders. Their coordinates were saved in ROI manager and applied to the initial image to measure the mean fluorescence intensity of the spots. Finally all the values were pooled and plotted as a frequency distribution plot (histogram).

Results and discussion

Synthesis

DBS fluorophores arose from the condensation of barbiturate dioxaborine **2** on three different 4-(diethylamino)benzaldehydes bearing various substituent at the *meta* position (Figure 1A). The obtained DBS fluorophores are thus composed of an aniline donor moiety and an acceptor barbiturate moiety linked through a double bond. The dioxaborine complex prevents the rotation of the acceptor and thus enhances the planarity of the π system leading to potentially bright fluorophores. Moreover, we showed recently that boron bridge renders a push-pull dioxaborine (DXB-Red) highly photostable in non-polar media.[49] The two cyclohexyl moieties were chosen for their hydrophobicity and bulkiness that can help in preventing formation of non-emissive *H*-aggregates by π-stacking.[50] [51] [52] Compared to DBS-H, an oxygen atom was introduced in DBS-OH in order to reinforce the electron density of the donor. This oxygen served to add an octyl hydrocarbon chain (DBS-C_8) in order to enhance the lipophilicity. The three DBS fluorophores were characterized by ^{1}H, ^{13}C and ^{19}F NMR as well as high-resolution mass spectroscopy (See SI). Additionally, X-ray diffraction of single crystal provided the crystallographic structure of DBS-C_8 that confirmed the coplanarity of the aniline and the barbituryl rings as well as the bulkiness brought by the two cyclohexyl moieties (figure 2B).

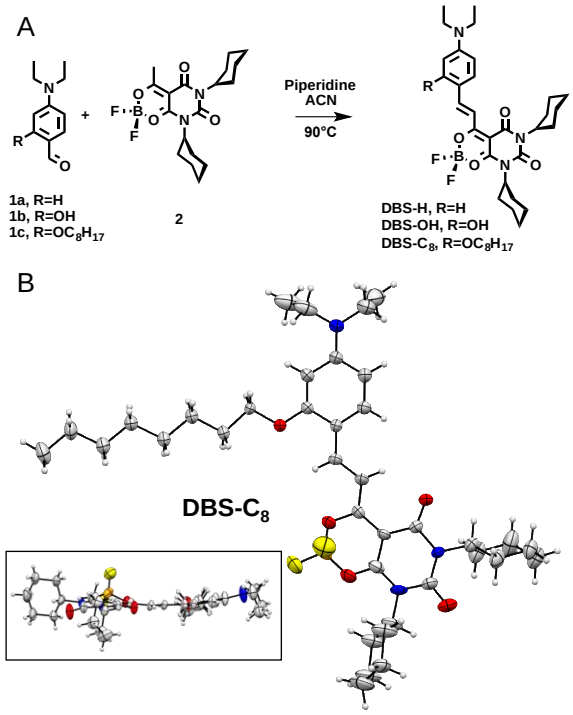

Figure 2. Synthesis of the DBS fluorophores (A) and ORTEP representation of DBS-C_8 obtained from X-ray diffraction (B), inset is the top view. For clarity, heteroatoms were colored: boron (orange), nitrogen (blue), oxygen (red) and fluorine (yellow).

Spectroscopic studies of DBS

The photophysical properties of DBS were first studied in various organic solvents with increasing polarity from cyclohexane to DMSO (all spectrum and values are available in figure S1, table S1). In non-polar solvent they are efficiently excitable at 488 nm, emit in the green-yellow range of the visible spectrum and possess quite similar absorption and emission maximum wavelengths with a slight red shift in emission when an additional oxygen atom on the aniline moiety was added (DBS-OH). DBS fluorophores showed a positive solvatochromism both in absorption and emission where bathochromic shifts occurred upon increase of solvent polarity (Figure 3, table 1). DBS-H displayed the highest solvatochromism with 39 nm and 71 nm in absorption and emission respectively. Nevertheless, when the maximum emission wavelengths of DBS dyes were plotted against the solvent polarity parameter $E_T(30)$, no linear correlation has been found (data not shown) indicating that other parameters such as the viscosity might influence their spectral properties. In compari-

son with styryl dyes,[53, 54] DBS dyes display shorter Stokes shifts ranging from 21 nm to 49 nm combined to sharper absorption and emission spectra (See FWHM values in table 1 and S1). Additionally, they possess high molar extinction coefficients ranging from 92,200 to 121,800 $M^{-1}.cm^{-1}$ in DMSO. Regarding the brightness, although DBS-H and DBS-C_8 displayed good quantum yields in toluene (0.62 and 0.50 respectively), quantum yields values in other solvents were generally modest to low (Table 1 and table S1).

Table 1. Photophysical properties of DBS dyes in cyclohexane and DMSO.

Dye	Solvent	λ_{Abs} (nm)	ε ($M^{-1}.cm^{-1}$)	FWHM Abs (nm)	λ_{Em} (nm)	FWHM Em (nm)	Stokes shift (nm)	ϕ [b] (QY)	Brightness [c] ($M^{-1}.cm^{-1}$)
DBS-H	Cyclohexane	508	78,000	50	521	32	13	0.13	10,100
	DMSO	548	98,400	74	592	66	44	0.04	3,900
DBS-OH	Cyclohexane[a]	513	67,200	58	542	37	29	0.20	13,400
	DMSO	551	94,000	60	579	59	28	0.03	2,800
DBS-C8	Cyclohexane	504	97,500	47	525	43	21	0.12	11,700
	DMSO	547	125,800	62	582	59	35	0.03	3,800

[a] Absorption spectra displayed a second peak at 526 nm.

[b] Quantum yields were measured using Rhodamine 6G in water (ϕ= 0.95) as a reference.

[c] Brightness is $\phi \times \varepsilon$.

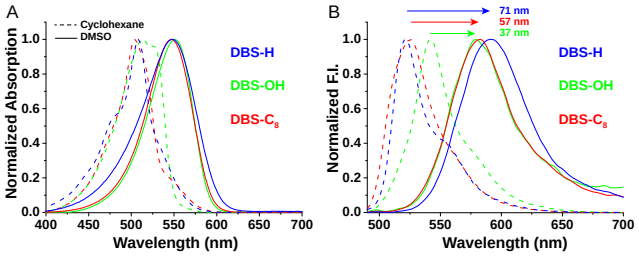

Figure 3. Normalized absorption (A) and emission (B) spectra of DBS (1 µM) in cyclohexane and DMSO. Excitation wavelength was 480 nm.

We then assessed the spectral properties of DBS in 9 different oils with various compositions and polarities and compared to NR668 (all spectrum and values are available in Figure S2 and Table S2). The results showed that maximum absorption wavelengths were all close to those obtained in EtOAc but with shorter emission wavelengths. Herein, we chose to focus on photophysical properties of DBS dyes obtained in medium chain triglycerides (MCT, Labrafac WL® 1349) as a representative and FDA approved oil, widely used in the formulation of parenteral emulsions,[23] and well represented in the low-energy nano-emulsification processes. Other types of oils outstandingly viscous castor oil and vitamin E acetate (VEA) also showed a very high brightness (see table S2). When compared to NR668, DBS dyes displayed a similar absorption maxima (~530 nm) and blue shifted emission (Figure 4 A-C). Importantly, absorption and emission bands of DBS dyes were significantly sharper in comparison to NR668 (Figure 4D-F). In addition, DBS dyes displayed equivalently high quantum yields but with ~2-fold larger molar extinction coefficients than NR668 (Table 2). Even though the molar extinction coefficients were slightly decreased in oils when compared to organic solvents, the quantum yields were much higher thus leading to a significant increase of brightness when dissolved in oils (Table 2).

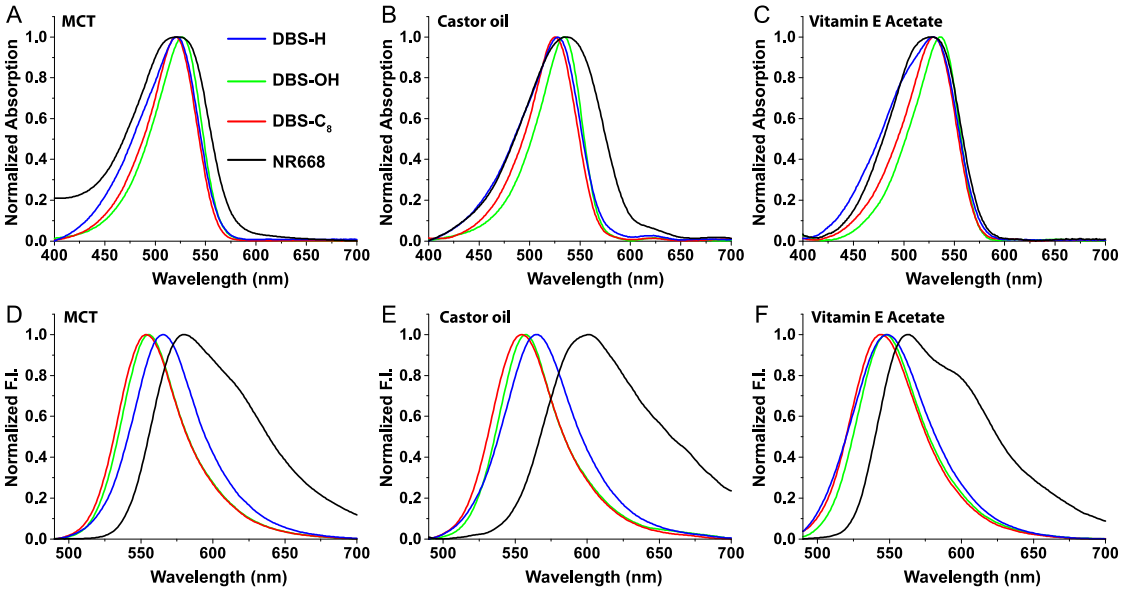

Figure 4. Normalized absorption (A, B, C) and emission (D, E, F) spectra of DBS dyes and NR668 in MCT (A, D), Castor oil (B, E) and VEA (C, F). Concentration was 1 µM. Excitation wavelength was 480 nm.

Similarly to the Statomerocyanines,[35] DBS form soluble aggregates in water that are non-emissive (data not shown). Therefore, DBS are fluorogenic dyes that undergo an impressive fluorescence enhancement from water to oil.

MCT, castor oil and VEA were detected as interesting candidates for the formulation of fluorescent NE, owing to the outstanding fluorescence properties of DBS when solubilized in these oils. To verify whether high QY values of DBS dyes in oils are related to theirs high viscosity, we studied the dependence of QY on dynamic viscosity η of the organic phase (solvent or oils). Results are reported in Figure S3, showing a linear correlation between the value of QY and log(η). The viscosity is known to enhance the quantum yield of dyes by restricting intramolecular rotational relaxation, which is commonly observed for so-called molecular rotors.[55] [56] This phenomenon is also known as "Motion-Induced Change in Emission" (MICE).[57] Our data showed that DBS fluorophores exhibit a molecular rotor behavior, which is in line with previously reported push-pull dioxaborine DXB-Red dye.[49] Interestingly, while the three DBS dyes showed very similar behavior (with similar fit slopes of 0.90, 0.97 and 0.92 for DBS-H, DBS-OH and DBS-C_8, respectively), NR668 did not disclose any trend, likely due to its highly solvatochromic nature thus being more sensitive to the polarity than to the viscosity. Altogether, the photo-physical features of DBS dyes, and this new sight on possibilities for optimizing their optical properties in those oils, constitute a promising system for the design of novel ultrabright NEs.

Table 2. Photophysical properties of DBS dyes in selected oils.

Dye	Oil	λ_{Abs} (nm)	ε ($M^{-1}.cm^{-1}$)	FWHM Abs (nm)	λ_{Em} (nm)	FWHM Em (nm)	Stokes shift (nm)	f [a] (QY)	Brightness [b] ($M^{-1}.cm^{-1}$)
DBS-H	MCT	521	76,300	68	566	54	45	0.42	32,000
	Castor oil	528	76,700	69	557	59	29	0.80	61,400
	VEA	257	59,100	81	548	63	21	0.62	36,600
DBS-OH	MCT	527	87,200	55	555	49	28	0.38	33,100
	Castor oil	534	98,400	54	559	49	25	0.87	85,600
	VEA	534	68,900	55	548	53	14	0.95	65,400
DBS-C8	MCT	520	102,300	56	554	51	34	0.48	49,100
	Castor oil	525	99,900	55	554	52	29	0.97	96,900
	VEA	527	80,200	60	544	56	17	0.86	69,000
NR668	MCT	525	40,100	87	593	84	58	0.98	39,300
	Castor oil	537	41,800	94	602	98	65	0.10	4,200
	VEA	525	41,400	79	563	85	38	0.86	35,600

[a] Quantum yields were measured using Rhodamine 6G in water (ϕ= 0.95) as a reference.

[b] Brightness is $\phi \times \varepsilon$.

Nano-emulsions

Considering the high performance of DBS dyes in oils, this system was selected for the formulation of fluorescent NEs. The simple methodology followed was a spontaneous nano-emulsification method designed with non-ionic PEGylated surfactant as water/oil interface stabilizer. [24, 25, 46, 58] The three oils mentioned above, related to the most efficient fluorescent properties of DBS, were formulated into NEs: *(i)* MCT: medium chain triglycerides (triglycerides composed of capric and caprylic acid), *(ii)* castor oil (composed of long chain C_{18} triglycerides), *(iii)* VEA (also known as tocopherol acetate), an acetylated phenol bearing a long branched aliphatic chain. As expected with spontaneous nano-emulsification,[46] the increase in the relative amount of non-ionic surfactant, decreased the NEs' mean size and polydispersity indexes (PDI) (assessed by dynamic light scattering, DLS, data Figure S4). However, significant differences in function of the oil used were noteworthy: while the castor oil systematically led to larger particles, MCT and VEA gave rise to similar size range, gradually decreasing from 185 nm to 22 nm as the ratio of surfactant (surfactant to oil weight ratio, SOR) was increased (Figure S4A). Interestingly, compared to MCT and castor oil, VEA NEs presented a significantly lower PDI independently of the surfactant/oil ratio (Figure S4B). This means that the emulsification protocol was much more efficient with this oil-surfactant couple.

In the second step, we determined the limit of solubility of the dyes in the oils, since it determines the maximum loading capacity of the NEs droplets, thus conditioning their maximum brightness. The results showed a quite important variability between the different conditions (Table S3), as the solubility varies from 0.3 wt.% to 7.6 wt.%. DBS-OH and DBS-H present relatively constant values whatever the nature of oil, around 2.7 wt.% and 4 wt.% respectively. This difference could be attributed to the difference of hydrophobicity between the DBS dyes. Indeed, the presence of the hydroxyl group in DBS-OH decreases its hydrophobicity and therefore decreases the solubility in oils compared to DBS-H. By contrast, solubility of DBS-C_8 showed a high variability: although it was poorly soluble in relatively polar MCT (maximum solubility 0.3 wt.%), it was well solubilized in castor oil (2.9 wt.%) and even better in VEA (7.6 wt.%). It follows therefrom that VEA oil provided the most interesting results, regarding *(i)* high quantum yields when solubilizing DBS dyes, *(ii)* high dye loading capability, *(iii)* smaller NEs with smaller PDI values. For these reasons, VEA was chosen to design DBS loaded fluorescent NEs, study and optimize the suspensions and evaluate their imaging properties in cellular imaging.

DBS loaded Fluorescent NE

The brightness of a nanoparticle (B) is defined by equation 1 where n is the number of loaded dye, ε is the molar extinction coefficient value of the loaded dye, and ϕ the quantum yield of the nanoparticle.[14]

$$\text{Eq. 1} \qquad B = n \times \varepsilon \times \phi$$

A simple way to increase the brightness of NEs would be to increase the number of fluorophores loaded in the oily core. Unfortunately, this approach is limited by the aggregation caused quenching (ACQ) provoked by the close proximity of the fluorophores.[14] This phenomenon leads to an important decrease of the NEs' quantum yield. In order to study fluorescent properties and brightness of NEs, and to compare the efficiency of DBS dyes and NR668 in providing bright NEs, we fixed the formulation parameters SOR = 50 wt.%, *i.e.* the droplet size around 50 nm (see Figure S4A), and then formulated different NEs, at different dye loading (ranging from 0.2 wt.% to 2.5 wt.% in oil). The sizes of the DBS-loaded and NR668-loaded NEs were very close (41.9 ± 3.3 nm and 44.5 ± 4.6 nm respectively) with very good PDI values < 0.09 (Figure 5A), showing that the emulsification process is robust and not affected by a slight modification of the oil composition. In order to assess the stability of the formed NEs over the time, their sizes were measured after 10 days. Results, reported in Table S4, suggested good stabilities of NEs, with exception of highly loaded DBS-H NEs, showing slight signs of size and PDI increase. To assess the ACQ phenomenon in this system, the quantum yields of the NEs were measured. The results showed that, globally, the quantum yields were quite different in function of the dyes (Figure 5B): DBS-OH appeared as less effective with a quantum yield starting at 0.50 which then underwent a fast drop upon increase of the dye loading. Compared to DBS-OH, DBS-H displayed much higher quantum yield values with a slower decrease upon dye loading. The best candidate was DBS-C_8 displaying high quantum yields at low loading (up to 0.91) and a quite high value of 0.44 at a loading as high as 2.5%, which corresponds to a concentration of 37 mM in oil. As a result, it seemed that the C_8 side arm (of DBS-C_8), in addition to enhancing the brightness of DBS in oils (Table 2), helps to prevent ACQ, probably by inducing a steric hindrance or a favorable spatial orientation.

Although NR668 provided descent QY values at high concentrations (Figure 5B) the formed NEs were less bright (Figure 5C) as the molar extinction coefficient ε of NR668 was about half of that of DBS dyes. Indeed, when the brightness per nano-droplet (calculated from the measured size and the values of QY and ε) was plotted *vs* dye loading, NEs loaded with DBS-H and especially DBS-C_8 appeared much brighter than those loaded with NR668 (Figure 5C). According to figure 5C, it appeared as a general trend that loadings superior to 1.5 wt.% did not provide brighter NEs as the brightness systematically decreased at higher loading.

In bioimaging, the photostability is of major importance especially for the tracking of fluorescent object over the time. For this purpose, NEs containing 1% of dyes were continuously irradiated and their fluorescence intensity was monitored over 1 hour (Figure 5D). Taken as reference, NR668 showed a relatively weak photostability as 65% of its fluorescence intensity was lost over 1h. On the other hand, DBS dyes globally displayed a much better photostability but some notable difference between each other. Once again the best results were obtained with DBS-C_8 that presented an impressive photostability, losing only 15% of its fluorescence intensity after 1 h photo-irradiation (Fig 5D).

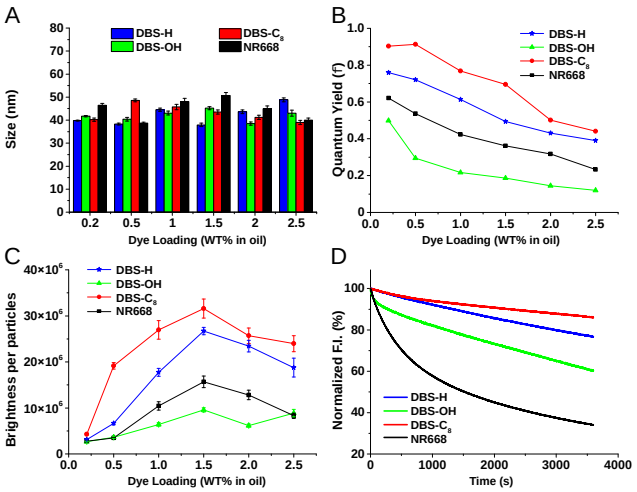

Figure 5. Characterization of dye-loaded VEA NEs. (A) Size of the NEs by DLS (diluted 100 times from formulation solution). (B) Quantum yields of NEs with increasing loading of dyes. (C) Brightness ($M^{-1}.cm^{-1}$) of single NEs calculated from equation 1 and according to the measured size. (D) Photostability of 1% dye-loaded NEs under continuous illumination (λ_{ex} were set to excite the fluorophores at the same ε value), fluorescence was monitored at 600 nm. The NEs were formulated in water. QY were obtained using rhodamine 6G as a reference (ϕ = 0.95 in water).

Given that DBS-C_8 displayed the highest brightness in NEs, the higher solubility in VEA and the best photostability, it was chosen for the next studies. In preparation of biological studies, next experiment was designed to evaluate the potential early leakage of the dye from the NEs to the biological media. Biomolecules, cells, tissues, contain many lipophilic domains (*e.g.* membranes or proteins) that can act as acceptor for the lipophilic dyes. Although DBS dyes were shown to have reduced brightness in non-viscous environments, in bioimaging experiments such dye leakage phenomenon can lead to decreasing of NEs brightness itself and thus enhancing the background noise.[21, 59]

In order to estimate the dye leakage, Fluorescent Correlation Spectroscopy (FCS) measurements were conducted in PBS alone and in the presence of 10 %(v/v) fetal bovine serum (FBS) (Table 3). Serum is an appropriate model of biological dye acceptor as it contains a high variety of amphiphilic biomolecules especially lipoproteins. We thus compared NR668 and DBS-C_8 loaded NEs with increasing dye-loading. First, the results confirmed the sizes obtained by DLS analysis and that DBS-C_8 loaded NEs were much brighter than the NR668 ones. Regarding the dye leakage, NR668 as well as DBS-C_8 loaded NEs showed limited leakage as the size and the concentration of fluorescent objects remained similar in the presence of 10% serum even at high dye-loading percentage (Table 3). At this stage of our work, cytotoxicity studies (MTT assay) were performed with the DBS dyes and NR668. The results showed no significant cytotoxicity up to 5 µM except for DBS-H that showed some sign of toxicity at 5 µM (Figure S5).

Table 3. Assessment of the dye leakage by fluorescent correlation spectroscopy (FCS).[a]

Dye	[Dye](%)	Solvent	τ (ms)	d (nm)	Brightness	[Droplets] (nM)
DBS-C_8	0.2	PBS	1.45	57.3	105	1.21
DBS-C_8	1.0	PBS	1.74	68.7	442	1.12
DBS-C_8	2.5	PBS	1.32	52.3	306	1.04
DBS-C_8	0.2	10% FBS	1.42	52.9	120	1.55
DBS-C_8	1.0	10% FBS	1.51	56.0	481	1.26
DBS-C_8	2.5	10% FBS	1.42	52.8	334	2.21
NR668	0.2	PBS	1.34	42.2	43.4	1.47
NR668	1.0	PBS	1.34	42.3	85.5	1.90
NR668	2.5	PBS	1.14	35.9	42.7	2.61
NR668	0.2	10% FBS	1.43	45.2	40.4	1.98
NR668	1.0	10% FBS	1.49	46.9	95.7	1.97
NR668	2.5	10% FBS	1.27	40.1	34.1	4.92

[a] τ (ms) – correlation time; d (nm) – hydrodynamic diameter; Brightness – brightness per particle with respect to reference (TMR); [Droplets] (nM) – concentration of nanodroplets. All measurements were done using TMR as reference.

Two-Photon imaging

Two-photon excitation (TPE) imaging possesses many advantages in bioimaging including limited photobleaching, lower phototoxicity, and reduced cell auto-fluorescence.[60, 61, 62] For these reasons, we investigated the two-photon absorption characteristics of DBS dyes. First, their TPE cross-section spectra in dioxane were measured (Figure 6A and S6) along with their quadratic intensity dependence (Figure S7). DBS dyes displayed similar spectra with two major excitation peaks at 980 nm and at 930 nm with absorption cross-section values between 430-734 GM and 76-130 GM, respectively. As a comparison NR668 has a weaker absorption (maximum at 980 nm, 140 GM) and displayed an additional peak at 810 nm (Figure S8A). In order to prove that these properties are conserved in NEs, TPE imaging was performed in live HeLa cells. Following our recently developed protocol,[34] we formulated

1% DBS-C_8 loaded NEs presenting negative charges (carboxylate groups) at the interface of nano-droplets to stimulate their internalization in the cells. After incubation with the NEs, the cells were imaged by TPE microscopy. Multicolor images with high signal-to-noise ratio were obtained showing that NEs were internalized by endocytosis (Figure 6B), which is in line with our previous studies.[34] As a control the same experiment was conducted with NR668, giving similar results (Figure S8B). These results demonstrated the compatibility of these new NEs with TPE imaging thus extending the choice in their imaging modality.

Altogether, these results prove that NEs arising from the combined use of DBS-C_8 dye with VEA oil lead to small and exceptionally bright lipid nanoparticles without non-specific interactions or leakage of the dye. Compared to our referenced dye NR668, DBS-C_8 presents important improvements namely: 1) sharper excitation and emission peaks, 2) enhanced photostability, 3) enhanced brightness and 4) higher two-photon absorption cross-section. All these features are important properties for bioimaging, especially for the tracking of individual NEs.

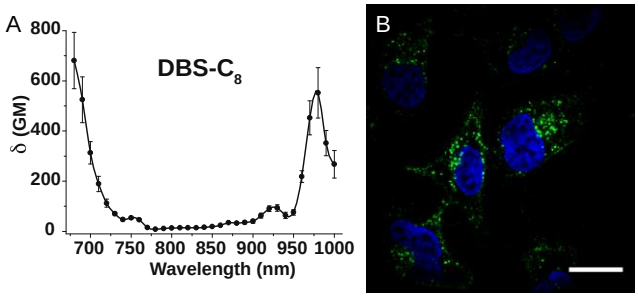

Figure 6. (A) Two-photon excitation cross-section spectra of DBS-C_8 in dioxane (18 μM). (B) Two-photon excitation imaging of HeLa cells incubated for 2 hours in the presence of NEs containing 1% PMAO and loaded with 1% DBS-C_8. Concentration of dye was set at 1 μM. Nucleus was stained with Hoechst (λ_{ex} = 930 nm). Scale bar is 10 μm.

Tracking of single NEs in cells

Aware of the advantageous features of our system, we undertook the tracking of single NEs in cells. Herein, the influence of the NEs' charge surface on their diffusion in the cytosol was studied as a model parameter to evidence the potential of this new bioimaging tool. Neutral NEs loaded with 1% DBS-C_8 (SOR = 50%) were prepared as well as exactly the same formulation with negatively charged surface using our described protocol.[34] After checking that both NEs had similar size (41 nm) and different zeta potentials (Table S5), they were micro-injected in HeLa cells at the same dye concentration (3 μM) and were imaged at various times after injection. To check that the same amount of NEs were microinjected in both case, the mean fluorescence of injected cells were measured and showed similar values of 647 ± 89 and 690 ± 110 (a.u.) for neutral and charged NEs respectively (quintuplicate experiment).

The analysis of recorded images evidenced clear differences in the distribution and mobility of the two types of NEs in the cytoplasm (Figure 7A-F). At 15 s post injection, the neutral NEs were distributed all over the cytoplasm with a gradient of intensity from the injection point (Figure 7E), whereas negatively charged NEs were mainly localized nearby the injection point (Figure 7B). Maximum intensity projection of movies acquired 5 min post-injection confirmed that neutral NEs reached the entire volume of the cytoplasm whereas negatively charged NEs remained confined to a restricted volume around the injection point probably due to non-specific interactions with biomolecules, membranes or organelles.

In the second step, this global observation was confirmed by individual tracking of NEs. Due to their intense brightness, high quality movies were obtained where individual NEs could be clearly distinguished with a high signal to noise ratio and minimal photobleaching (movie available in SI). For both NEs, individual particles were tracked and their trajectory and velocity in the cytoplasm have been determined (Figure 7G and Figure S9). Although PEGylated NEs were already shown to be prevented from aggregation in complex media,[24, 25] the distribution of their mean fluorescence intensity was first plotted in order to prove that NEs did not aggregate in the cytosol of the cells (Figure S10). The results presented in a histogram (Figure 7H) showed first that the majority of the NEs moves with a relatively low velocity, lower than 1 μm.s^{-1}. Then, it is noteworthy that neutral NEs display higher velocities compared to negatively-charged ones. Indeed, above 0.8 μm.s^{-1} the proportion of neutral NEs is systematically higher than the negatively charged ones and below this value, this tendency reverses. Among all velocities measured for the displacements of negatively charged NE, only 30% were higher than 0.8 μm.s^{-1}, while this fraction represents 46% for the neutral ones. These results showed that the charges at NEs interface influence their mobility in the cytoplasm. Presumably, in comparison to neutral NEs, negatively charged NEs are more likely to be involved in non-specific interactions with biomolecules such as free proteins or those anchored in organelles, thus slowing down their progression.

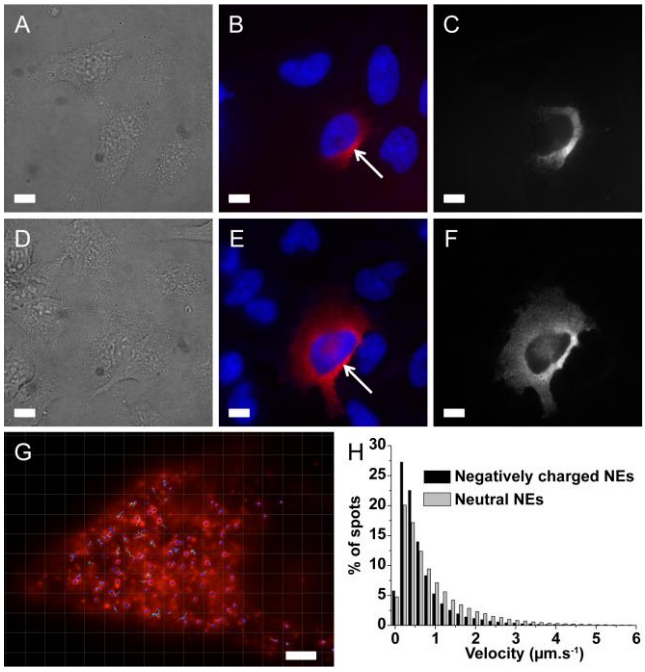

Figure 7. Micro-injection of NEs (41 nm) in HeLa cells and their individual tracking. Images of HeLa cells microinjected with negatively charged NEs (A-C) and neutral NEs (D-F). (A, D) Transmission light microscopy 5 min after injection. (B, E) Epifluorescence imaging 15 s post injection; the NEs are in red and the nu-

clei are in blue (Hoechst 5 μg/mL); white arrows indicate the injection point. (C, F) NEs' maximum intensity projection of a 30 s time laps (50 ms acquisition time, total of 600 images), 5 min post injection. Scale bar is 10 μm. (G) Example of a HeLa cell microinjected with neutral NEs where single NEs have been spotted (blue spots) and their trajectory tracked using Imaris 9.2.1 (Bitplane Inc) software, scale bar is 3 μm. (H) Histogram of NEs' velocity in the cytosol obtained by individual NEs' tracking from movies right after injection (30 s, 50 ms acquisition time).

Conclusion

In this work we introduced DBS dyes, a new family of lipophilic and neutral styryl fluorophores that are composed of a barbituryl dioxaborine acceptor moiety and different aniline donor groups. In addition to their fluorescence enhancement from solvents to viscous oils, these dyes display improved properties compared to the previously used fluorophore NR668 including an enhanced brightness and photostability, a higher two-photon absorption and sharper peaks. With the prospection of using these new fluorescent and lipophilic molecules in the formulation of NEs, we proposed in this study to screen the main physicochemical parameters and establish a relationship between the fluorescence properties and physicochemical properties of the NEs. After evaluating their photophysical properties in various oils, we found that NEs composed of vitamin E acetate as the lipid core loaded with DBS bearing an octyl chain (DBS-C_8) led to small NEs (-40 nm) with low polydispersity index. Additionally, they displayed the highest brightness and photostability with no leakage of the dye out of the particle. These NEs were used in TPE imaging and in microinjection experiments in HeLa cells. Thanks to their superior fluorescent properties we obtained movies that allowed the tracking of individual NEs. We were able to demonstrate significant differences in the NEs' velocity when spreading in the cytosol dependent on their interface charges. The combination of their interesting photophysical properties and their two-photon absorption might make DBS dyes suitable for tracking individual NEs in tissues or *in vivo* experiments. We believe that this system will contribute in extending the knowledge on lipid nano-droplets and nanoparticles and their interactions with biological environments.

AUTHOR INFORMATION

*Corresponding Authors

- nanton@unistra.fr
- andrey.klymchenko@unistra.fr
- mayeul.collot@unistra.fr

Author Contributions

The manuscript was written through contributions of all authors. MC synthesized and characterized the DBS dyes. XW performed the emulsions and all the spectroscopic experiments and measurements. HA tracked the single particles. PA measured the two-photon absorption and performed the TPE imaging. MC performed the microinjection and imaging. TKF assessed the cytotoxicity. NA, ASK and MC supervised the work and wrote the manuscript. TV contributed to materials and analysis tools. All authors have given approval to the final version of the manuscript.

Funding Sources

This work was supported by ERC Consolidator grant BrightSens 648528 and ANR BrightRiboProbes (ANR-16-CE11-0010). XW was founded by the China Scholarship Council PhD fellowship (CSC No. 201706240033).

ACKNOWLEDGMENT

We acknowledge Dr. Delphine Garnier from the Service de Chimie Analytique (SCA) for her assistance in the LC-MS and RMN analyses and Dr. Lydia for the crystallographic data.

ASSOCIATED CONTENT

Supporting Information

The Supporting Information is available free of charge on the ACS Publications website. It contains: Synthesis protocol, NMR and mass caracterizations of the compounds, tables with photophysical properties in various media, emission spectra, stability tests, solubility of DBS in oils, characterizations of emulsions as well as cytotoxicity assays and two-photon absorbance.

Microinjection of DBS-C_8 loaded NEs (Supplementary movie, AVI)

REFERENCES

(1) Pelaz, B.; Alexiou, C.; Alvarez-Puebla, R.A.; Alves, F.; Andrews, A.M.; Ashraf, S.; Balogh, L.P.; Ballerini, L.; Bestetti, A.; Brendel, C.; Bosi, S.; Carril, M.; Chan, W.C.W.; Chen, C.; Chen, X.; Chen, X.; Cheng, Z.; Cui, D.; Du, J.; Dullin, C.; Escudero, A.; Feliu, N.; Gao, M.; George, M.; Gogotsi, Y.; Grünweller, A.; Gu, Z.; Halas, N.J.; Hampp, N.; Hartmann, R.K.; Hersam, M.C.; Hunziker, P.; Jian, J.; Jiang, X.; Jungebluth, P.; Kadhiresan, P.; Kataoka, K.; Khademhosseini, A.; Kopeček, J.; Kotov, N.A.; Krug, H.F.; Lee, D.S.; Lehr, C.-M.; Leong, K.W.; Liang, X.-J.; Ling Lim, M.; Liz-Marzán, L.M.; Ma, X.; Macchiarini, P.; Meng, H.; Möhwald, H.; Mulvaney, P.; Nel, A.E.; Nie, S.; Nordlander, P.; Okano, T.; Oliveira, J.; Park, T.H.; Penner, R.M.; Prato, M.; Puntes, V.; Rotello, V.M.; Samarakoon, A.; Schaak, R.E.; Shen, Y.; Sjöqvist, S.; Skirtach, A.G.; Soliman, M.G.; Stevens, M.M.; Sung, H.-W.; Tang, B.Z.; Tietze, R.; Udugama, B.N.; VanEpps, J.S.; Weil, T.; Weiss, P.S.; Willner, I.; Wu, Y.; Yang, L.; Yue, Z.; Zhang, Q.; Zhang, Q.; Zhang, X.-E.; Zhao, Y.; Zhou, X.; Parak, W.J. Diverse Applications of Nanomedicine. *ACS Nano* **2017**, *11* (3), 2313–2381. https://doi.org/10.1021/acsnano.6b06040.

(2) Liong, M.; Lu, J.; Kovochich, M.; Xia, T.; Ruehm, S. G.; Nel, A. E.; Tamanoi, F.; Zink, J. I. Multifunctional Inorganic Nanoparticles for Imaging, Targeting, and Drug Delivery. *ACS Nano* **2008**, *2* (5), 889–896. https://doi.org/10.1021/nn800072t.

(3) Peng, H.-S.; Chiu, D. T. Soft Fluorescent Nanomaterials for Biological and Biomedical Imaging. *Chem. Soc. Rev.* **2015**, *44* (14), 4699–4722. https://doi.org/10.1039/C4CS00294F.

(4) Kunjachan, S.; Ehling, J.; Storm, G.; Kiessling, F.; Lammers, T. Noninvasive Imaging of Nanomedicines and Nanotheranostics: Principles, Progress, and Prospects. *Chem. Rev.* **2015**, *115* (19), 10907–10937. https://doi.org/10.1021/cr500314d.

(5) Li, Z.; Barnes, J. C.; Bosoy, A.; Stoddart, J. F.; Zink, J. I. Mesoporous Silica Nanoparticles in Biomedical Applications. *Chem. Soc. Rev.* **2012**, *41* (7), 2590–2605. https://doi.org/10.1039/c1cs15246g.

(6) Tang, F.; Li, L.; Chen, D. Mesoporous Silica Nanoparticles: Synthesis, Biocompatibility and Drug Delivery. *Adv. Mater. Deerfield Beach Fla* **2012**, *24* (12), 1504–1534. https://doi.org/10.1002/adma.201104763.

(7) Zhou, J.; Yang, Y.; Zhang, C. Toward Biocompatible Semiconductor Quantum Dots: From Biosynthesis and Bioconjugation to Biomedical Application. *Chem. Rev.* **2015**, *115* (21), 11669–11717. https://doi.org/10.1021/acs.chemrev.5b00049.

(8) Laurent, S.; Forge, D.; Port, M.; Roch, A.; Robic, C.; Vander Elst, L.; Muller, R. N. Magnetic Iron Oxide Nanoparticles: Synthesis, Stabilization, Vectorization, Physicochemical Characterizations, and Biological Applications. *Chem. Rev.* **2008**, *108* (6), 2064–2110. https://doi.org/10.1021/cr068445e.

(9) Astruc, D.; Boisselier, E.; Ornelas, C. Dendrimers Designed for Functions: From Physical, Photophysical, and Supramolecular Properties to Applications in Sensing, Catalysis, Molecular Electronics, Photonics, and Nanomedicine. *Chem. Rev.* **2010**, *110* (4), 1857–1959. https://doi.org/10.1021/cr900327d.

(10) Lee, C. C.; MacKay, J. A.; Fréchet, J. M. J.; Szoka, F. C. Designing Dendrimers for Biological Applications. *Nat. Biotechnol.* **2005**, *23* (12), 1517–1526. https://doi.org/10.1038/nbt1171.

(11) Kumari, A.; Yadav, S. K.; Yadav, S. C. Biodegradable Polymeric Nanoparticles Based Drug Delivery Systems. *Colloids Surf. B Biointerfaces* **2010**, *75* (1), 1–18. https://doi.org/10.1016/j.colsurfb.2009.09.001.

(12) Elsabahy, M.; Wooley, K. L. Design of Polymeric Nanoparticles for Biomedical Delivery Applications. *Chem. Soc. Rev.* **2012**, *41* (7), 2545–2561. https://doi.org/10.1039/c2cs15327k.

(13) Delplace, V.; Couvreur, P.; Nicolas, J. Recent Trends in the Design of Anticancer Polymer Prodrug Nanocarriers. *Polym. Chem.* **2014**, *5* (5), 1529–1544. https://doi.org/10.1039/C3PY01384G.

(14) Reisch, A.; Klymchenko, A. S. Fluorescent Polymer Nanoparticles Based on Dyes: Seeking Brighter Tools for Bioimaging. *Small Weinh. Bergstr. Ger.* **2016**, *12* (15), 1968–1992. https://doi.org/10.1002/smll.201503396.

(15) Kamaly, N.; Yameen, B.; Wu, J.; Farokhzad, O. C. Degradable Controlled-Release Polymers and Polymeric Nanoparticles: Mechanisms of Controlling Drug Release. *Chem. Rev.* **2016**, *116* (4), 2602–2663. https://doi.org/10.1021/acs.chemrev.5b00346.

(16) Torchilin, V. P. Recent Advances with Liposomes as Pharmaceutical Carriers. *Nat. Rev. Drug Discov.* **2005**, *4* (2), 145–160. https://doi.org/10.1038/nrd1632.

(17) Mehnert, W.; Mäder, K. Solid Lipid Nanoparticles: Production, Characterization and Applications. *Adv. Drug Deliv. Rev.* **2001**, *47* (2–3), 165–196.

(18) Anton, N.; Vandamme, T. F. The Universality of Low-Energy Nano-Emulsification. *Int. J. Pharm.* **2009**, *377* (1–2), 142–147. https://doi.org/10.1016/j.ijpharm.2009.05.014.

(19) McClements, D. J. Nanoemulsions versus Microemulsions: Terminology, Differences, and Similarities. *Soft Matter* **2012**, *8* (6), 1719–1729. https://doi.org/10.1039/C2SM06903B.

(20) Yao, M.; Xiao, H.; McClements, D. J. Delivery of Lipophilic Bioactives: Assembly, Disassembly, and Reassembly of Lipid Nanoparticles. *Annu. Rev. Food Sci. Technol.* **2014**, *5*, 53–81. https://doi.org/10.1146/annurev-food-072913-100350.

(21) Klymchenko, A. S.; Roger, E.; Anton, N.; Anton, H.; Shulov, I.; Vermot, J.; Mely, Y.; Vandamme, T. F. Highly Lipophilic Fluorescent Dyes in Nano-Emulsions: Towards Bright Non-Leaking Nano-Droplets. *RSC Adv.* **2012**, *2* (31), 11876–11886. https://doi.org/10.1039/C2RA21544F.

(22) Li, X.; Anton, N.; Zuber, G.; Vandamme, T. Contrast Agents for Preclinical Targeted X-Ray Imaging. *Adv. Drug Deliv. Rev.* **2014**, *76*, 116–133. https://doi.org/10.1016/j.addr.2014.07.013.

(23) Anton, N.; Hallouard, F.; Attia, M. F.; Vandamme, T. F. Nano-Emulsions for Drug Delivery and Biomedical Imaging. In *Intracellular Delivery III: Market Entry Barriers of Nanomedicines*; Prokop, A., Weissig, V., Eds.; Fundamental Biomedical Technologies; Springer International Publishing: Cham, 2016; pp 273–300. https://doi.org/10.1007/978-3-319-43525-1_11.

(24) Li, X.; Anton, N.; Zuber, G.; Zhao, M.; Messaddeq, N.; Hallouard, F.; Fessi, H.; Vandamme, T. F. Iodinated α-Tocopherol Nano-Emulsions as Non-Toxic Contrast Agents for Preclinical X-Ray Imaging. *Biomaterials* **2013**, *34* (2), 481–491. https://doi.org/10.1016/j.biomaterials.2012.09.026.

(25) Attia, M. F.; Anton, N.; Chiper, M.; Akasov, R.; Anton, H.; Messaddeq, N.; Fournel, S.; Klymchenko, A. S.; Mély, Y.; Vandamme, T. F. Biodistribution of X-Ray Iodinated Contrast Agent in Nano-Emulsions Is Controlled by the Chemical Nature of the Oily Core. *ACS Nano* **2014**, *8* (10), 10537–10550. https://doi.org/10.1021/nn503973z.

(26) Kilin, V. N.; Anton, H.; Anton, N.; Steed, E.; Vermot, J.; Vandamme, T. F.; Mely, Y.; Klymchenko, A. S. Counterion-Enhanced Cyanine Dye Loading into Lipid Nano-Droplets for Single-Particle Tracking in Zebrafish. *Biomaterials* **2014**, *35* (18), 4950–4957. https://doi.org/10.1016/j.biomaterials.2014.02.053.

(27) Texier, I.; Goutayer, M.; Da Silva, A.; Guyon, L.; Djaker, N.; Josserand, V.; Neumann, E.; Bibette, J.; Vinet, F. Cyanine-Loaded Lipid Nanoparticles for Improved in Vivo Fluorescence Imaging. *J. Biomed. Opt.* **2009**, *14* (5), 054005-054005-11. https://doi.org/10.1117/1.3213606.

(28) Bouchaala, R.; Mercier, L.; Andreiuk, B.; Mély, Y.; Vandamme, T.; Anton, N.; Goetz, J. G.; Klymchenko, A. S. Integrity of Lipid Nanocarriers in Bloodstream and Tumor Quantified by Near-Infrared Ratiometric FRET Imaging in Living Mice. *J. Controlled Release* **2016**, *236*, 57–67. https://doi.org/10.1016/j.jconrel.2016.06.027.

(29) Ma, X.; Sun, R.; Cheng, J.; Liu, J.; Gou, F.; Xiang, H.; Zhou, X. Fluorescence Aggregation-Caused Quenching versus Aggregation-Induced Emission: A Visual Teaching Technology for Undergraduate Chemistry Students. *J. Chem. Educ.* **2016**, *93* (2), 345–350. https://doi.org/10.1021/acs.jchemed.5b00483.

(30) Lainé, A.-L.; Gravier, J.; Henry, M.; Sancey, L.; Béjaud, J.; Pancani, E.; Wiber, M.; Texier, I.; Coll, J.-L.; Benoit, J.-P.; Passirani, C. Conventional versus Stealth Lipid Nanoparticles: Formulation and in Vivo Fate Prediction through FRET Monitoring. *J. Control. Release Off. J. Control. Release Soc.* **2014**, *188*, 1–8. https://doi.org/10.1016/j.jconrel.2014.05.042.

(31) Reisch, A.; Didier, P.; Richert, L.; Oncul, S.; Arntz, Y.; Mély, Y.; Klymchenko, A. S. Collective Fluorescence Switching of Counterion-Assembled Dyes in Polymer Nanoparticles. *Nat. Commun.* **2014**, *5*, 4089. https://doi.org/10.1038/ncomms5089.

(32) Huang, Y.; Zhang, G.; Hu, F.; Jin, Y.; Zhao, R.; Zhang, D. Emissive Nanoparticles from Pyridinium-Substituted Tetraphenylethylene Salts: Imaging and Selective Cytotoxicity towards Cancer Cells in Vitro and in Vivo by Varying Counter Anions. *Chem. Sci.* **2016**, *7* (12), 7013–7019. https://doi.org/10.1039/C6SC02395A.

(33) Greenspan, P.; Mayer, E. P.; Fowler, S. D. Nile Red: A Selective Fluorescent Stain for Intracellular Lipid Droplets. *J. Cell Biol.* **1985**, *100* (3), 965–973. https://doi.org/10.1083/jcb.100.3.965.

(34) Attia, M. F.; Dieng, S. M.; Collot, M.; Klymchenko, A. S.; Bouillot, C.; Serra, C. A.; Schmutz, M.; Er- Rafik, M.; Vandamme, T. F.; Anton, N. Functionalizing Nanoemulsions with Carboxylates: Impact on the Biodistribution and Pharmacokinetics in Mice. *Macromol. Biosci.* **2017**, *17* (7), 1600471. https://doi.org/10.1002/mabi.201600471.

(35) Collot, M.; Fam, T. K.; Ashokkumar, P.; Faklaris, O.; Galli, T.; Danglot, L.; Klymchenko, A. S. Ultrabright and Fluorogenic Probes for Multicolor Imaging and Tracking of Lipid Droplets in Cells and Tissues. *J. Am. Chem. Soc.* **2018**. https://doi.org/10.1021/jacs.7b12817.

(36) Pfister, A.; Zhang, G.; Zareno, J.; Horwitz, A. F.; Fraser, C. L. Boron Polylactide Nanoparticles Exhibiting Fluorescence and Phosphorescence in Aqueous Medium. *ACS Nano* **2008**, *2* (6), 1252–1258. https://doi.org/10.1021/nn7003525.

(37) Contreras, J.; Xie, J.; Chen, Y. J.; Pei, H.; Zhang, G.; Fraser, C. L.; Hamm-Alvarez, S. F. Intracellular Uptake and Trafficking of Difluoroboron Dibenzoylmethane−Polylactide Nanoparticles in HeLa Cells. *ACS Nano* **2010**, *4* (5), 2735–2747. https://doi.org/10.1021/nn901385y.

(38) Kerr, C.; DeRosa, C. A.; Daly, M. L.; Zhang, H.; Palmer, G. M.; Fraser, C. L. Luminescent Difluoroboron β-Diketonate PLA–PEG Nanoparticle. *Biomacromolecules* **2017**, *18* (2), 551–561. https://doi.org/10.1021/acs.biomac.6b01708.

(39) Magde, D.; Rojas, G. E.; Seybold, P. G. Solvent Dependence of the Fluorescence Lifetimes of Xanthene Dyes. *Photochem. Photobiol.* **1999**, *70* (5), 737–744. https://doi.org/10.1111/j.1751-1097.1999.tb08277.x.

(40) Albota, M. A.; Xu, C.; Webb, W. W. Two-Photon Fluorescence Excitation Cross Sections of Biomolecular Probes from 690 to 960 Nm. *Appl. Opt.* **1998**, *37* (31), 7352–7356.

(41) Clamme, J. P.; Azoulay, J.; Mély, Y. Monitoring of the Formation and Dissociation of Polyethylenimine/DNA Complexes by Two Photon Fluorescence Correlation Spectroscopy. *Biophys. J.*

2003, *84* (3), 1960–1968. https://doi.org/10.1016/S0006-3495(03)75004-8.

(42) Spingler, B.; Schnidrig, S.; Todorova, T.; Wild, F. Some Thoughts about the Single Crystal Growth of Small Molecules. *CrystEngComm* **2012**, *14* (3), 751–757. https://doi.org/10.1039/C1CE05624G.

(43) "M86-E01078 APEX2 User Manual", Bruker AXS Inc., Madison, USA, 2006.

(44) Sheldrick, G. M. Phase Annealing in SHELX-90: Direct Methods for Larger Structures. *Acta Crystallogr. A* **1990**, *46* (6), 467–473. https://doi.org/10.1107/S0108767390000277.

(45) Sheldrick, G. M. A Short History of SHELX. *Acta Crystallogr. A* **2008**, *64* (1), 112–122. https://doi.org/10.1107/S0108767307043930.

(46) Anton, N.; Vandamme, T. F. The Universality of Low-Energy Nano-Emulsification. *Int. J. Pharm.* **2009**, *377* (1), 142–147. https://doi.org/10.1016/j.ijpharm.2009.05.014.

(47) Reisch, A.; Heimburger, D.; Ernst, P.; Runser, A.; Didier, P.; Dujardin, D.; Klymchenko, A. S. Protein-Sized Dye-Loaded Polymer Nanoparticles for Free Particle Diffusion in Cytosol. *Adv. Funct. Mater.* **2018**, *28* (48), 1805157. https://doi.org/10.1002/adfm.201805157.

(48) Müller, P.; Schwille, P.; Weidemann, T. PyCorrFit-Generic Data Evaluation for Fluorescence Correlation Spectroscopy. *Bioinforma. Oxf. Engl.* **2014**, *30* (17), 2532–2533. https://doi.org/10.1093/bioinformatics/btu328.

(49) Karpenko, I. A.; Niko, Y.; Yakubovskyi, V. P.; Gerasov, A. O.; Bonnet, D.; Kovtun, Y. P.; Klymchenko, A. S. Push-Pull Dioxaborine as Fluorescent Molecular Rotor: Far-Red Fluorogenic Probe for Ligand-Receptor Interactions. *J. Mater. Chem. C* **2016**, *4* (14), 3002–3009. https://doi.org/10.1039/C5TC03411F.

(50) Gieseking, R. L.; Mukhopadhyay, S.; Risko, C.; Marder, S. R.; Brédas, J.-L. Effect of Bulky Substituents on Thiopyrylium Polymethine Aggregation in the Solid State: A Theoretical Evaluation of the Implications for All-Optical Switching Applications. *Chem. Mater.* **2014**, *26* (22), 6439–6447. https://doi.org/10.1021/cm5028755.

(51) Frischmann, P. D.; Würthner, F. Synthesis of a Non-Aggregating Bay-Unsubstituted Perylene Bisimide Dye with Latent Bromo Groups for C–C Cross Coupling. *Org. Lett.* **2013**, *15* (18), 4674–4677. https://doi.org/10.1021/ol401946g.

(52) Ozdemir, T.; Atilgan, S.; Kutuk, I.; Yildirim, L. T.; Tulek, A.; Bayindir, M.; Akkaya, E. U. Solid-State Emissive BODIPY Dyes with Bulky Substituents As Spacers. *Org. Lett.* **2009**, *11* (10), 2105–2107. https://doi.org/10.1021/ol9005568.

(53) Rosania, G. R.; Lee, J. W.; Ding, L.; Yoon, H.-S.; Chang, Y.-T. Combinatorial Approach to Organelle-Targeted Fluorescent Library Based on the Styryl Scaffold. *J. Am. Chem. Soc.* **2003**, *125* (5), 1130–1131. https://doi.org/10.1021/ja027587x.

(54) Yan, P.; Acker, C. D.; Zhou, W.-L.; Lee, P.; Bollensdorff, C.; Negrean, A.; Lotti, J.; Sacconi, L.; Antic, S. D.; Kohl, P.; Mansvelder, H.D., Pavone, F.S., Loew, L.M. Palette of Fluorinated Voltage-Sensitive Hemicyanine Dyes. Proc. Natl. *Acad. Sci. U. S. A.* **2012**, *109* (50), 20443–20448. https://doi.org/10.1073/pnas.1214850109.

(55) Kuimova, M. K. Mapping Viscosity in Cells Using Molecular Rotors. *Phys. Chem. Chem. Phys. PCCP* **2012**, *14* (37), 12671–12686. https://doi.org/10.1039/c2cp41674c.

(56) Haidekker, M. A.; Theodorakis, E. A. Molecular Rotors--Fluorescent Biosensors for Viscosity and Flow. *Org. Biomol. Chem.* **2007**, *5* (11), 1669–1678. https://doi.org/10.1039/b618415d.

(57) Su, D.; Teoh, C. L.; Wang, L.; Liu, X.; Chang, Y.-T. Motion-Induced Change in Emission (MICE) for Developing Fluorescent Probes. *Chem. Soc. Rev.* **2017**, *46* (16), 4833–4844. https://doi.org/10.1039/C7CS00018A.

(58) Li, X.; Anton, N.; Ta, T. M. C.; Zhao, M.; Messaddeq, N.; Vandamme, T. F. Microencapsulation of nanoemulsions: novel Trojan particles for bioactive lipid molecule delivery https://www.dovepress.com/microencapsulation-of-nanoemulsions-novel-trojan-particles-for-bioacti-peer-reviewed-article-IJN (accessed Oct 19, 2018). https://doi.org/10.2147/IJN.S20353.

(59) Bouchaala, R.; Anton, N.; Anton, H.; Vandamme, T.; Vermot, J.; Smail, D.; Mély, Y.; Klymchenko, A. S. Light-Triggered Release from Dye-Loaded Fluorescent Lipid Nanocarriers in Vitro and in Vivo. *Colloids Surf. B Biointerfaces* **2017**, *156*, 414–421. https://doi.org/10.1016/j.colsurfb.2017.05.035.

(60) Helmchen, F.; Denk, W. Deep Tissue Two-Photon Microscopy. *Nat. Methods* **2005**, *2* (12), 932–940. https://doi.org/10.1038/nmeth818.

(61) Svoboda, K.; Yasuda, R. Principles of Two-Photon Excitation Microscopy and Its Applications to Neuroscience. *Neuron* **2006**, *50* (6), 823–839. https://doi.org/10.1016/j.neuron.2006.05.019.

(62) Piston, D. W. Imaging Living Cells and Tissues by Two-Photon Excitation Microscopy. *Trends Cell Biol.* **1999**, *9* (2), 66–69. https://doi.org/10.1016/S0962-8924(98)01432-9.

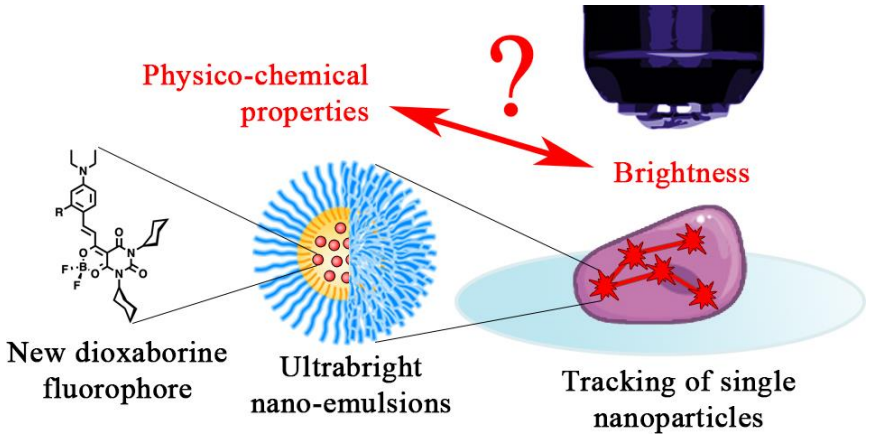

For TOC only